Theory and Design of a Tapered Line Distributed Photodetector

Jin-Wei Shi and Chi-Kuang Sun, *Senior Member, IEEE*

***Abstract*—We present the theory and design of a tapered line distributed photodetector (TLDP). In the previously demonstrated velocity-matched distributed photodetector (VMDP), high electrical bandwidth is achieved by proper termination in the input end to absorb reverse traveling waves, sacrificing one-half of the quantum efficiency. By utilizing the tapered line structure and phase matching between optical waves and microwaves in our analyzed structure, a traveling-wave photodetector is more realizable and ultrahigh bandwidth can be attained due to removal of the extra input dummy load that sacrifices one-half of the total quantum efficiency.**

To investigate the advantages of TLDP over VMDP, we calculate their electrical bandwidth performances by using an analytic photodistributed current model. We adopted low-temperature-grown (LTG) GaAs-based metal–semiconductor–metal (MSM) traveling-wave photodetectors as example unit active devices in the analytic bandwidth calculation for their high-speed and high-power performances. Both VMDP and TLDP in our simulation are assumed to be transferred onto glass substrates, which would achieve high microwave velocity/impedance and make radiation loss negligible. The simulated bandwidth of a properly designed LTG GaAs MSM TLDP is ∼325 GHz, which is higher than the simulated bandwidth of the LTG GaAs MSM VMDP with an open-circuit input end (∼240 GHz) and is almost comparable to the simulated bandwidth of an input-terminated LTG GaAs MSM VMDP (∼330 GHz). This proposed method can be applied to the design of high-bandwidth distributed photodetectors for radio-frequency photonic systems and optoelectronic generation of high-power microwaves and millimeter waves.

***Index Terms*—Distributed photodetector, high-bandwidth photodetector, high-power photodetector, low-temperature-grown GaAs, metal–semiconductor–metal (MSM) photodetector, tapered line, traveling-wave photodetector, ultra-high-speed photodetector, velocity-matched distributed photodetector.**

I. Introduction

TWO MAJOR trends in the development of ultra-high-speed photodetectors (PDs) are improving bandwidth-efficiency product and obtaining high output saturation power [1]. Regarding the latter, the most direct way is to reduce the optical modal absorption constant and increase the device absorption volume or length [2], [3]. However, the electrical bandwidth will decrease significantly for the case of long-absorption-length PDs [2]–[4] due to serious high-frequency microwave loss and velocity mismatch or R-C bandwidth limitations. A velocity-matched distributed photodetector (VMDP) structure is one way to improve the power-bandwidth product, which distributes the optical power in each downscaled high-speed PD and collects the photocurrent from each PD by a low-loss electrical transmission line to reduce the microwave loss and improve the output power. Its high electrical bandwidth and high saturation power performance have also been demonstrated [5]. However, for a VMDP structure, in order to absorb the reverse traveling microwave and eliminate the traditional R-C bandwidth limitation, additional dummy load in the input end is needed. This input termination will sacrifice one-half of the quantum efficiency and increase the dark current when high dc bias voltage is applied to get high output power. On the other hand, the input-matching load is usually removed for real applications and high-power measurements [5], [6]. Without the input-matching load in a VMDP, it will behave like an all-lump-type device due to oscillations of reverse traveling microwaves inside the structure of the long distributed PD. Velocity matching between optical waves and microwaves is thus no longer a useful condition in the improvement of device electrical bandwidth [4].

In this paper, we present the theory and design procedures of a modified traveling-wave distributed photodetector: tapered line distributed photodetector (TLDP). By gradually changing the characteristic impedance of the interconnected coplanar-waveguide (CPW) lines between adjacent unit active PDs, the reverse traveling wave can be canceled [7]. High-speed performance can thus be achieved without sacrificing half of the quantum efficiency in the input dummy load.

To compare the electrical bandwidth performance with that of an ordinary VMDP, we adopt an analytical photodistributed current model to simulate the electrical bandwidth performance of TLDPs and VMDPs. We use the low-temperature-grown (LTG) GaAs-based metal–semiconductor–metal (MSM) traveling-wave photodetector (TWPD) [8] as an example unit PD in the bandwidth calculations for both distributed PD structures due to its high-speed and high-power performances [8]. Both types of distributed PDs in our simulation are assumed to be transferred onto glass substrates [9] to reduce radiation loss. Low dielectric constant of glass substrate will ensure that the fabricated electrical transmission lines have higher characteristic impedance and microwave velocity than those on an ordinary GaAs substrate and eliminate most radiation loss in high-impedance lines [10], [11]. High microwave velocity thus achieved will also reduce the propagation delay between different active unit PDs and increase the Bragg cutoff frequency of the artificial transmission line [12]. By properly designing the structure of a TLDP to achieve phase matching

Manuscript received January 16, 2002; revised July 11, 2002. This work was supported by the National Science Council of Taiwan under Grant NSC 89-2215-E-002-064 and the National Science Foundation of USA under Award INT-9813411.

The authors are with the Department of Electrical Engineering and the Graduate Institute of Electro-Optical Engineering, National Taiwan University, Taipei, Taiwan, R.O.C. (e-mail: sun@cc.ee.ntu.edu.tw).

Digital Object Identifier 10.1109/JLT.2002.806331

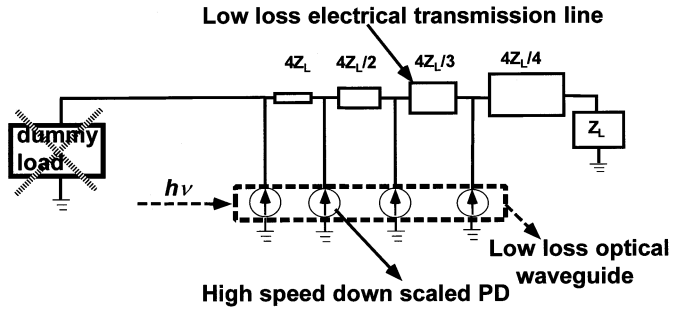

Fig. 1. Conceptual diagram of TLDP structure. Z_L is the impedance value of the load termination. Dashed and solid lines represent optical and electrical paths, respectively.

between microwaves and optical waves, the simulated electrical bandwidth of the modeled TLDP is ∼325 GHz, which is much higher than the simulated bandwidth (∼240 GHz) of a comparison input-open VMDP due to the tapered line distributed connection structure. Compared with the previous theoretical work in tapered line distributed photodetectors [13], we not only propose an equivalent circuit model, which can get more physical insight into the working principles of the TLDP, but also present detailed design and simulation procedures, which are analytic and intuitive to demonstrate the feasibility and advantages of TLDP structure.

II. Device Structure and Design Concept

The conceptual diagram of a TLDP structure is shown in Fig. 1. Each current source on an optical waveguide represents a downscaled high-speed PD, such as a uni-traveling-carrier-photodetector (UTC-PD) [14], [15], an LTG GaAs-based p-i-n TWPD [16], an MSM PD [5], or a p-i-n PD [17], which feeds its generated photocurrent into an electrical transmission line. The low-loss optical waveguide should be designed for distributing the input optical power and reducing the scattering loss between different active PDs. To distribute the optical power in each PD equally and avoid the saturation in the first PD, the optical waveguide could also be replaced by a multimode interference optical power splitter as in previously demonstrated VMDPs [6], [18]. The major difference of TLDPs from VMDPs is the structure of the electrical transmission line, which collects the photocurrent from each unit PD. Different widths of transmission line in different tapered sections represent different characteristic impedances. For the case of a 50-Ω system with four tapered stages, the impedances of different tapered sections are 200 Ω, 100 Ω (200/2 Ω), 66.67 Ω (200/3 Ω), and 50 Ω (200/4 Ω), respectively. The impedance mismatch between different tapered sections will induce a backward out-of-phase reflection wave, which will cancel the reverse traveling wave in each active photoabsorption region. A detailed explanation is given in [7], [12], and [19].

On the other hand, a tapered line structure can be viewed as a simplified structure of a power combing circuit, and various impedance values in different tapered sections originating from a different number of transmission lines are parallel-combined in each section. In this paper, by utilizing an equivalent circuit model, we can obtain more physical insight into the working

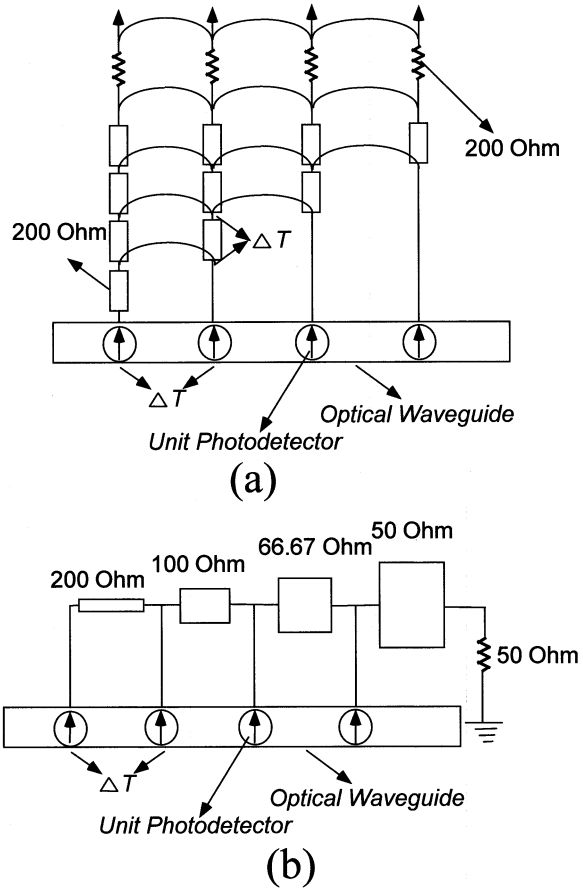

Fig. 2. (a) Equivalent circuit model and (b) its simplified version of TLDP circuit structure. Each rectangle represents one section of transmission line, which has a characteristic impedance of 200 Ω. ΔT is the time interval for optical waves traveling through one optical waveguide section, which is the same as the time interval for microwaves passing one section of transmission line.

principles of the proposed tapered line structure, which is shown in Fig. 2(a) and (b). Each current source in Fig. 2 represents an active photoabsorption region. We assumed that the generated currents from different active regions are the same by properly designing the area of each active region. The most direct way to eliminate the reverse traveling wave without sacrificing output current in distributed PDs or distributed electrical amplifiers is to collect the generated current from each unit active device (PD or amplifier) by its own electrical transmission line [20]–[22] and to terminate with a 200-Ω characteristic impedance, as shown in Fig. 2(a). By eliminating a common power combining electrical transmission line, where the collected current from each unit device can propagate in both forward and backward directions, the reverse traveling wave problem can be eliminated. However, in order to combine the power from each separate electrical transmission line, an extra broadband and low-loss power combing passive circuit topology is usually needed [20], [21], which is lossy, complex, impractical, and inconvenient. This problem can be solved by simplifying and replacing Fig. 2(a) with a tapered line structure, as shown in Fig. 2(b), which has a single 50-Ω output port.

The simplification of Fig. 2(a) begins with properly designing the structures and lengths of electrical transmission lines and optical waveguides. Thus the propagation time

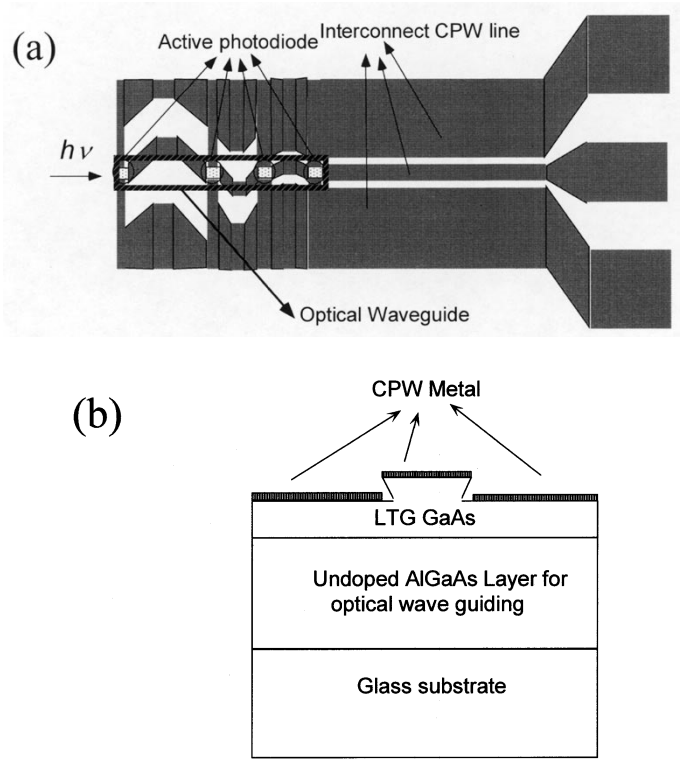

Fig. 3. (a) Top view of an example TLDP and (b) cross-sectional diagram of its active region.

ΔT for microwaves passing one section of the electrical transmission line and the propagation time for optical waves traveling through one section of the optical waveguide can be equivalent. Therefore, the phases and magnitudes of the photogenerated microwave signals in the connected points between different electrical transmission lines can be the same, as shown in Fig. 2(a). Then Fig. 2(a) can be simplified by equal potential point connection. The resulting tapered line structure equivalent circuit is found in Fig. 2(b), which shows different values of characteristic impedance due to different numbers of transmission line sections for parallel combination in each tapered section. According to the above discussion about the working principle of a TLDP, we can clearly know that the most important goals in the detailed design of a TLDP are 1) to make the photocurrent from each unit PD the same and 2) to achieve the required tapered impedance value with phase matching between microwaves and optical waves in each distributed section simultaneously.

To simulate the TLDP structure and compare the electrical bandwidth performance with the untapered VMDP, we adopted the LTG GaAs-based MSM TWPD as an example unit active PD in our bandwidth calculation for its high-speed and high-output power characteristics [8], [23], [24]. The proposed example structure of a TLDP and its cross-sectional diagram in the active photoabsorption region (MSM TWPD) are shown in Fig. 3(a) and (b), respectively. The challenge in designing the tapered line structure is the high impedance line of the first tapered section [12], [19]–[21]. A high impedance line will cause high radiation loss in the case of a CPW transmission line, especially in the desired high-frequency regime (hundreds of gigahertz) due to wide air gaps [10], [11]. To overcome and neglect the radiation loss problem, the TLDP is assumed to be transferred onto a glass substrate, as shown in Fig. 3(b), which has a low dielectric constant; the capacitance of the interconnect lines can thus be reduced significantly. A high impedance line with negligible radiation loss in the first tapered section could thus be achieved [10], [11].

We suggest that the velocity-matching condition between optical waves and microwaves in previous VMDPs could be replaced by phase matching in our proposed TLDP structure. This phase matching could be achieved by properly designing the lengths of optical and microwave waveguides, because optical mode velocity in semiconductor (GaAs) is much lower than microwave velocity in glass substrates, which have low effective dielectric constants and capacitance for high-impedance purposes. As shown in Fig. 3(a), unit MSM TWPDs are located on a straight optical waveguide. The longer length of the winding interconnect CPW line compared with the straight optical waveguide is due to higher microwave velocity compared with optical wave velocity. The bending in interconnected CPW lines is also usually encountered in practical circuits [12], [25] and causes excess capacitance, which might affect the performance as well as the bandwidth of the desired circuits. Usually chamfered bends or rounded corners [25] are used to compensate for this nonideal effect, especially in a 90° bending [25]–[27]. We did not consider this minor nonideal effect in our proposed example TLDP structure, which can be minimized in the real design and fabrication process by chamfering the bend and reducing the bending angles ($\sim$50°).

The design of a TLDP begins with determining the total absorption length and optical confinement factor in the leaky optical waveguide. Then, we can design the length of each absorption active region (for example, MSM TWPD) to obtain the same amount of output photocurrents from every active region. The chosen parameters of an example TLDP structure are given in Table I. After determining each absorption length, we can decide the lengths of the microwave waveguide and optical waveguide to achieve the required tapered impedance value and phase-matching condition simultaneously. The length of interconnect microwave waveguide in each tapered section is determined by the required characteristic impedance Z_L, which is given by [5]

$$Z_L = \sqrt{\frac{L_{\text{line}}}{C_{\text{line}} + \frac{C_{\text{self}} \times l_a}{l_e}}} \tag{1}$$

where L_{line} and C_{line} are the per-unit-length inductance and capacitance of the interconnect CPW line. C_{self} and l_a are the per-unit-length capacitance and length of the MSM TWPD. l_e is the required electrical spacing between adjacent tapered sections. The values of C_{self} and C_{line} can be calculated from velocity equations with [28]

$$\begin{aligned} \frac{c}{\sqrt{\varepsilon_{\text{self}}}} &= \frac{1}{\sqrt{L_{\text{self}} C_{\text{self}}}} \\ \frac{c}{\sqrt{\varepsilon_{\text{line}}}} &= \frac{1}{\sqrt{L_{\text{line}} C_{\text{line}}}} \end{aligned} \tag{2}$$

TABLE I
SIMULATION PARAMETERS OF TLDP AND VMDP STRUCTURES. THE LISTED GEOMETRY PARAMETERS (LENGTHS AND WIDTHS) OF DIFFERENT DISTRIBUTED SECTIONS ARE ARRANGED FROM INPUT ENDS TOWARD OUTPUT PORTS OF THE DEVICES

	TLDP	VMDP
Center strip width and air gap of MSM TWPD active region	2μm/0.3μm	2μm/0.3μm
Center strip widths of each connected distributed sections	2μm, 5μm, 6μm	10μm
CPW air gap of each connected distributed sections	130μm, 60μm, 45μm	17μm
Ground plane width	50 μm	50 μm
Metal (Ti/Au) thickness	1 μm	1 μm
Interconnected optical waveguide lengths between distributed sections (include device absorption lengths of MSM TWPD)	35μm, 20μm, 15μm	15μm
Interconnected CPW lengths between distributed sections	60μm, 20μm, 15μm	15μm
Device absorption length of each MSM TWPD	4μm, 5.5μm, 8.5μm, 15μm	9μm
AlGaAs/GaAs epi layer thickness	5μm	5μm
Microwave dielectric constant of AlGaAs/GaAs epi layers	12	12
Microwave dielectric constant of glass substrate	2.25	2.25
Optical modal absorption constant $\Gamma\alpha$ (μm^{-1})	0.06	0.06
Group velocity of optical wave	$8.71\times10^7\, m/\sec$	$8.71\times10^7\, m/\sec$
Carrier lifetime (t_{life})	200 fs	200 fs

where c is the light speed in vacuum. $\varepsilon_{\rm self}$ and $\varepsilon_{\rm line}$ are the effective dielectric constants of the active MSM region and interconnect CPW transmission line region, respectively, which depend on the geometric size of the CPW line and the thickness of different layers in a membrane substrate. The exact calculation formulas are given in [29]. The values of inductance $L_{\rm line}$ and $L_{\rm self}$ can be determined by the empirical formulas [30]. Take one of the tapered sections—for example, the value of Z_L is known. Then we can determine the value of l_e by properly choosing a reasonable ratio between the width of the center metal strip and the air gap in both interconnect CPW and MSM regions for calculating the required values of $C_{\rm line}$, $C_{\rm self}$ and $L_{\rm line}$, $L_{\rm self}$ as discussed before. After obtaining the value of l_e, we can further determine the length of each optical waveguide l_o to achieve phase matching between optical waves and microwaves as discussed before. The geometry size of the whole TLDP structure can be determined by utilizing the optical/electrical phase-matching condition with

$$l_e\sqrt{L_{\rm line}\left(C_{\rm line}+\frac{C_{\rm self}\times l_a}{l_e}\right)}=\frac{l_o}{V_o} \tag{3}$$

where V_o is the optical propagation velocity, which is about 8.7 $\times$ 10^7 m/s in a GaAs-based optical waveguide [5].

III. BANDWIDTH SIMULATION RESULTS

Generally speaking, the electrical bandwidth of a distributed PD is limited by the cutoff frequencies of unit PDs, Bragg cutoff frequency of the artificial electrical transmission line

[12], [31], microwave loss/dispersion, and transit and lifetimes of the photogenerated carriers [5]. To specify the advantages of TLDP over VMDP, we simulated the bandwidth of both structures by developing a photodistributed current model [4]. The basic concept and principle of this model has been used in the bandwidth calculation of fully distributed TWPDs [4] and distributed amplifier circuits [28]. The accuracy of our adopted design procedures and simulation concepts has already been verified by the previous measurement results of ultra-high-speed PDs, such as traveling-wave distributed PDs [15] and fully distributed TWPDs [4], [16]. Compared with the traditional ABCD matrix model [5], this model is simple, analytic, and allows physical insight into the working principles of the distributed structures.

Fig. 4 shows the conceptual diagram of an artificial electrical transmission line with four periodic loading current sources "A," "B," "C," and "D," which we use in the bandwidth calculation of a VMDP. The microwave velocity and characteristic impedance of this artificial transmission line can be determined from (1) and (3), which are accurate in our case because the spacing between each unit PD (tens of micrometers) is small compared with the simulated wavelength (hundreds to thousands micrometers) [5].

Microwave loss is composed of conductor loss, radiation loss, and dielectric loss [25]. We neglected the radiation loss in our simulation because it is quite small in our proposed membrane substrate structure [11]. Equations (4) and (5) represent the generated forward and backward photocurrents from each distributed PD to the output load for the case of a VMDP

$$\begin{aligned} I_f(\omega) = {} & \frac{P_a}{2} \times (\exp(-\gamma_m \times (m_{la}+m_{lb}+m_{lc}))) \\ & + \frac{P_b}{2} \times (\exp(-\gamma_m \times (m_{lb}+m_{lc}))) \\ & \times (\exp(-j \times \beta_o \times l_{oa})) \\ & + \frac{P_c}{2} \times (\exp(-\gamma_m \times (m_{lc}))) \\ & \times (\exp(-j \times \beta_o \times (l_{oa}+l_{ob}))) \\ & + \frac{P_d}{2} \times (\exp(-j \times \beta_o \times (l_{oa}+l_{ob}+l_{oc}))) \qquad (4) \end{aligned}$$

$$\begin{aligned} I_b(\omega) = {} & \frac{P_a}{2} \times (\exp(-\gamma_m \times (m_{la}+m_{lb}+m_{lc}))) \\ & + \frac{P_b}{2} \times (\exp(-\gamma_m \times (m_{la} \times 2+m_{lb}+m_{lc}))) \\ & \times (\exp(-j \times \beta_o \times l_{oa})) \\ & + \frac{P_c}{2} \times (\exp(-\gamma_m \times (2 \times (m_{la}+m_{lb})+m_{l_c}))) \\ & \times (\exp(-j \times (\beta_o \times (l_{oa}+l_{ob})))) \\ & + \frac{P_d}{2} \times (\exp(-\gamma_m \times (2 \times (m_{la}+m_{lb}+m_{l_c})))) \\ & \times (\exp(-j \times (\beta_o \times (l_{oa}+l_{ob}+l_{oc})))). \qquad (5) \end{aligned}$$

$I_f(\omega)$ and $I_b(\omega)$ are the forward and backward propagation photocurrents, respectively. γ_m is the microwave propagation constant, which can be determined by (1), (3), and microwave propagation loss. P_a, P_b, P_c, and P_d are the fractions of total generated photocurrent, which is normalized to one, from each unit PD. The values of these parameters can be determined by optical modal absorption constant ($\Gamma\alpha$) and the absorption length of each unit PD. The factor 0.5 in front of these parameters represents one-half of the photocurrent forward and backward propagating toward the load and input end, respectively. β_o is the propagation constant of the modulated optical wave envelope. We neglected the optical propagation loss between adjacent unit PDs, which is quite small ($\sim$0.1 dB/cm) in a well-designed optical waveguide [5], [32]. m_{la}, m_{lb}, and m_{lc} are the lengths of the interconnected CPW lines between adjacent unit PDs. l_{oa}, l_{ob}, and l_{oc} are the section lengths of optical waveguides, which include device absorption lengths of unit MSM TWPD and the lengths of interconnected optical waveguides. In the case of the VMDP structure, propagation constants of optical waves and microwaves are similar; thus these six parameters must be the same to achieve phase matching between optical wave and microwave.

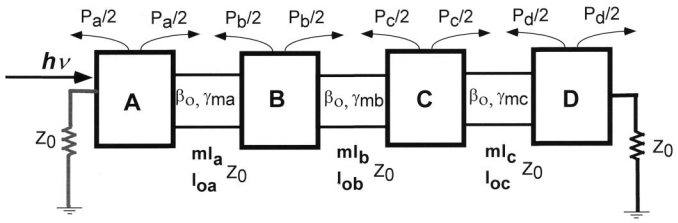

Fig. 4. Conceptual diagram of a VMDP, which is used in the photodistributed current-model calculation. The dummy load in the input end is removed for the bandwidth simulation of the open-circuit VMDP.

These two equations can be understood as follows. Taking the term $P_c/2$ in (4), for example, as shown in Fig. 4, the term $\exp(-j \times \beta_o \times (l_{oa} + l_{ob}))$ represents the excitation phase of $P_c/2$, which originates from the propagation phase shift of optical waves traveling through two sections of waveguides and two device absorption lengths (l_{oa} and l_{ob}). The term $\exp(-\gamma_m \times (m_{lc}))$ represents the phase shift of microwaves, which travel from unit PD "C" to the load. By multiplying these terms, we can obtain the complete frequency response function of the "C" current source. With the same concept, we can obtain frequency response functions of A, B, and D in (4). With respect to (5), we can clearly see that the transfer functions of the unit PD "A," "B," "C," and "D" in this equation are similar to their corresponding terms of optical phase shift in (4). On the other hand, the forms of electrical phase shift are different due to the nature of backward propagation. Take the term $P_c/2$ in (5), for example. $\exp(-\gamma_m \times (2 \times (m_{la} + m_{lb}) + m_{lc}))$ represents the backward propagation microwaves from the unit PD "C," which must travel through the interconnected CPW lines m_{la} and m_{lb} twice and then propagate through m_{lc} to the termination load due to the bouncing of the backward propagation waves from the open-circuit termination in the input end of the whole PD.

In the case of VMDPs with an impedance-matching termination in the input end of the device, backward propagation microwaves are eliminated. Thus the electrical bandwidth can just be modeled by (4). In the case of VMDPs with an open-circuit termination in the input end, their electrical bandwidth per-

formance can be modeled through the summations of (4) and (5). To obtain the device electrical bandwidth and amplitude responses for both cases, we multiply the obtained current response I_n with the frequency response of an exponential-like carrier lifetime of LTG GaAs, the cutoff frequency of each unit PD (MSM-TWPD), and the Bragg cutoff frequency [12], [31].

The detailed and complete transfer functions used in bandwidth calculation are shown in (6) and (7) for the case of VMDPs with and without input impedance-matching termination, respectively

$$I_n(\omega) = I_f(\omega) \times \frac{1}{1+j\omega t_{\text{life}}} \times \frac{1}{1+j\frac{\omega}{\omega_c}} \times \frac{1}{1+j\frac{\omega}{\omega_B}} \tag{6}$$

$$I_n(\omega) = (I_f(\omega) + I_b(\omega)) \times \frac{1}{1+j\omega t_{\text{life}}} \times \frac{1}{1+j\frac{\omega}{\omega_c}} \times \frac{1}{1+j\frac{\omega}{\omega_B}}. \tag{7}$$

t_{life} is the carrier lifetime of LTG GaAs, which is about 200 fs [33], and ω_c is the cutoff frequency of the MSM TWPD, which can be calculated using a photodistributed current model with boundary reflection effects [4]. ω_B is the Bragg cutoff angular frequency in each section of the artificial electrical transmission line, which is given as follows [31]:

$$\omega_B = \frac{2}{\sqrt{L_{\text{total}} C_{\text{total}}}} \tag{8}$$

where L_{total} and C_{total} are the total capacitance and inductance in each section of the artificial electrical transmission line. We can rewrite its form as in (9) to get more physical insight

$$\omega_B = \frac{2}{\sqrt{L_{\text{total}} C_{\text{total}}}} = \frac{2}{\sqrt{LC}\, l_e} \cong \frac{2V_e}{l_e} = \frac{2}{\tau_e} \tag{9}$$

where L and C are the values of per-unit-length inductance and capacitance and l_e is the length of the transmission line between two unit PDs. Thus the Bragg cutoff frequency can be treated as the inverse of microwave propagation delay (τ_e) between two unit PDs.

To simulate our example TLDP structure, the photodistributed current model must be modified. The complete equations for forward $(I_f(\omega))$ and backward $(I_b(\omega))$ propagating microwaves are given in (10) and (11)

$$\begin{aligned}
I_{f1}(\omega) &= P_a \times \exp(-\gamma_{ma} \times m_{la}) \times T_1 \times \exp(-\gamma_{mb} \times m_{lb}) \\
&\quad \times T_2 \times \exp(-\gamma_{mc} \times m_{lc}) \times T_3 \\
I_{f2}(\omega) &= D_{f1} \times P_b \times \exp(-j \times \beta_o \times l_{oa}) \times \exp(-\gamma_{mb} \times m_{lb}) \\
&\quad \times T_2 \times \exp(-\gamma_{mc} \times m_{lc}) \times T_3 \\
I_{f3}(\omega) &= D_{f2} \times P_c \times \exp(-j \times \beta_o \times (l_{oa} + l_{ob})) \\
&\quad \times \exp(-\gamma_{mc} \times m_{lc}) \times T_3 \\
I_{f4}(\omega) &= D_{f3} \times P_d \times \exp(-j \times \beta_o \times (l_{oa} + l_{ob} + l_{oc})) \\
I_f(\omega) &= I_{f1}(\omega) + I_{f2}(\omega) + I_{f3}(\omega) + I_{f4}(\omega)
\end{aligned} \tag{10}$$

$$\begin{aligned}
I_{b1}(\omega) &= P_a \times \exp(-\gamma_{ma} \times m_{la}) \times R_1 + D_{b1} \times P_b \\
&\quad \times \exp(-j \times \beta_o \times l_{oa}) \\
I_{b2}(\omega) &= P_a \times \exp(-\gamma_{ma} \times m_{la}) \times T_1 \times \exp(-\gamma_{mb} \times m_{lb}) \\
&\quad \times R_2 + D_{f1} \times P_b \times \exp(-\gamma_{mb} \times m_{lb}) \\
&\quad \times \exp(-j \times \beta_o \times l_{oa}) \times R_2 + D_{b2} \times P_c \\
&\quad \times \exp(-j \times \beta_o \times (l_{oa} + l_{ob})) \\
I_{b3}(\omega) &= P_a \times \exp(-\gamma_{ma} \times m_{la}) \times T_1 \times \exp(-\gamma_{mb} \times m_{lb}) \\
&\quad \times T_2 \times \exp(-\gamma_{mc} \times m_{lc}) \times R_3 + D_{f1} \times P_b \\
&\quad \times \exp(-\gamma_{mb} \times m_{lb}) \times \exp(-j \times \beta_o \times l_{oa}) \times T_2 \\
&\quad \times \exp(-\gamma_{mc} \times m_{lc}) \times R_3 + D_{f2} \times P_c \\
&\quad \times \exp(-\gamma_{mc} \times m_{lc}) \times \exp(-j \times \beta_o \times (l_{oa} + l_{ob})) \\
&\quad \times R_3 + D_{b3} \times P_d \times \exp(-j \times \beta_o \times (l_{oa} + l_{ob} + l_{oc})) \\
I_b(\omega) &= I_{b1}(\omega) + I_{b2}(\omega) + I_{b3}(\omega).
\end{aligned} \tag{11}$$

We neglect the infinite reflections between open-circuit input end and load termination of $I_b(\omega)$ in (11) because it is almost canceled and just occupies a small fraction ($\sim$ 0.01) of the total generated photocurrent $(I_n(\omega) = I_b(\omega) + I_f(\omega))$ in a well-designed tapered line structure, as discussed later. γ_{ma}, γ_{mb}, γ_{mc}, γ_{md} correspond to the microwave propagation constants in different sections of the tapered electrical transmission lines. Their lengths are m_{la}, m_{lb}, m_{lc}, and m_{ld}, respectively. T_1, T_2, T_3 and R_1, R_2, R_3 are the transmission and reflection coefficients in each connected point between adjacent sections of the tapered transmission line and distributed photocurrent sources, as shown in Fig. 5(a). D_{fn}, D_{bn} $(n = 1 \sim 3)$ are the ratios of forward and backward propagation photocurrents to the total generated current in each unit PD. These ratios depend on the values of impedances between two connected sections.

Equations (10) and (11) can be understood as follows. By utilizing the superposition principle, the forward propagating current $I_f(\omega)$ in (10) can be decomposed to four terms $I_{f1}(\omega)$, $I_{f2}(\omega)$, $I_{f3}(\omega)$, $I_{f4}(\omega)$, which correspond to the generated photocurrents from sources "A," "B," "C," "D," as shown in Fig. 5(a). Similarly, the total backward propagating current $I_b(\omega)$ can be obtained by summing the contributions from connected points between "AB," "BC," and "CD" as $I_{b1}(\omega)$, $I_{b2}(\omega)$, and $I_{b3}(\omega)$.

Fig. 5(b) and the inset of Fig. 5(a) show conceptual example diagrams of how to determine the values of T_n, R_n, D_{fn}, and D_{bn} $(n = 1 \sim 3)$ [7], [12], [13]. We assumed that the amount of generated photocurrent in each current source is I_p by properly designing the length of each active PD as shown in Fig. 5(b). The first current source will inject all of I_p into the line section with Z_0 due to the unterminated input end. When this wave reaches the next line section with $Z_0/2$, the current reflection coefficient R_1 will be $-1/3$. In accordance with Kirchhoff's law, a current of $4/3I_p$ will flow into the next section, which implies that the transmission coefficient T_1 equals

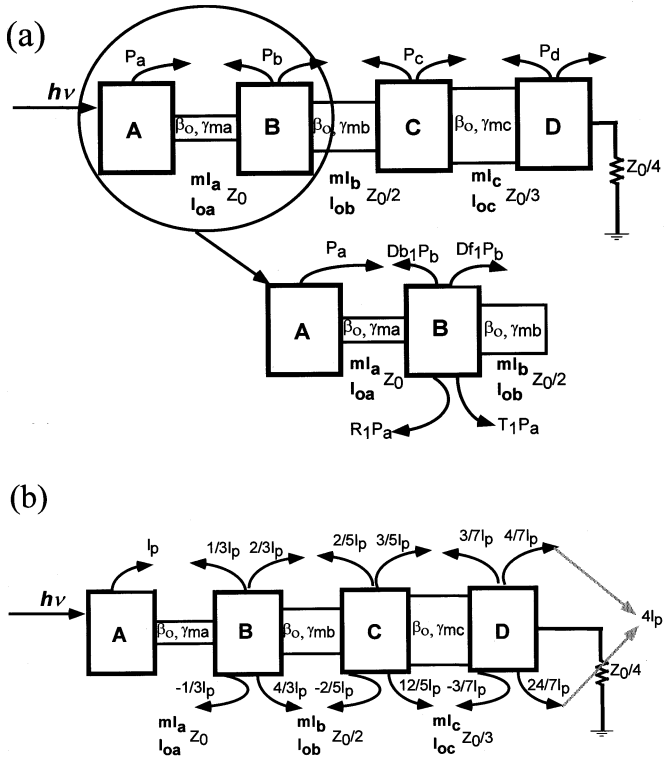

Fig. 5. (a) Conceptual diagram of a TLDP, which is used in photodistributed current-model calculation. (b) Conceptual diagram for current summation process in a TLPD structure. The inset in (a) illustrates how to determine the reflection (R_1), transmission (T_1), and division coefficients (D_{f1}, D_{b1}).

4/3. The second current source will split its current between the two sections based on the relative impedance. One-third of the current will travel toward the input and two-thirds toward the output. Thus the values of D_{f1} and D_{b1} are 2/3 and 1/3, respectively. $D_{b1}I_p$ exactly cancels the R_1I_p from the reflected incident wave, while $D_{f1}I_p$ adds with the transmitted wave for a full $2I_p$. The process is repeated at the next two current sources with a suitable choice of line impedances $Z_0/3$ and $Z_0/4$. The values of $R_{2\sim3}$, $T_{2\sim3}$, and $D_{f2\sim3}$, $D_{b2\sim3}$ can be determined as follows: $-1/5(R_2)$, $-1/7(R_3)$, $6/5(T_2)$, $8/7(T_3)$ and $3/5(D_{f2})$, $4/7(D_{f3})$, $2/5(D_{b2})$, $3/7(D_{b3})$, respectively. The magnitudes of generated photocurrents $I_{f1\sim f3}(\omega)$ can thus be determined.

In (10) and (11), moreover, if the phase between optical waves and microwaves in each tapered section is synchronized by utilizing (3) as discussed before. We can let

$$\gamma_{ma\sim c} \times m_{la\sim c} \cong j \times \beta_o \times l_{oa\sim c} = j \times \omega\tau \qquad (12)$$

by assuming low microwave loss, where τ is the propagation delay of optical waves or microwaves. Therefore, we can simplify (10) and (11) and get

$$I_f(\omega) \cong 4I_p \times \exp(-3 \times j \times \omega\tau)$$
$$I_b(\omega) \cong I_{b1}(\omega) \cong I_{b2}(\omega) \cong I_{b3}(\omega) \cong 0. \qquad (13)$$

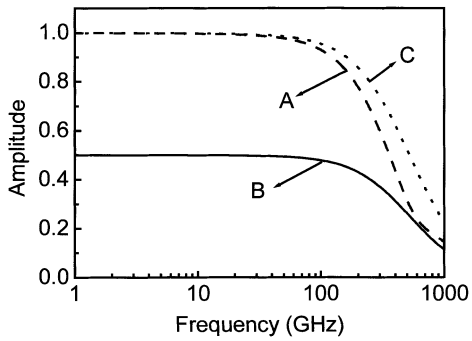

Fig. 6. The simulated current response of open-circuit VMDP (trace A, dashed line), input-terminated VMDP (trace B, solid line), and TLDP (trace C, dotted line).

The results obtained in (13) are similar to those in (4) except that twice the amount of collected photocurrent can be obtained. Its conceptual diagram is shown in Fig. 5(b). From (10)–(13), we can know that the key point of success in TLDP structure is phase matching between optical waves and microwaves, properly choosing the impedance value in each connected transmission line, and the length of each unit PD.

To quantify the advantage of the tapered structure, the frequency responses of VMDPs with open circuit input end and proper input termination have been compared with the TLDP. The frequency response of the simulated TLDP structure can be obtained by (4)–(7), (10), and (11). However, here we neglect the Bragg cutoff frequencies (~1 THz) in different distributed sections, which could be much higher than the obtained electrical bandwidth (~300 GHz), by shortening the lengths of the interconnected CPW lines (less than 50 μm) and reducing the microwave propagation delay. Both structures are designed for 50-Ω impedances with the same stage numbers, the same kind of active unit PD (MSM TWPD), and the same total length of active devices, which is the summed lengths of four active unit PDs, as well as on similar glass substrates.

All of the detailed parameters used in electrical bandwidth simulation are given in Table I. The simulated frequency responses of current amplitudes are shown in Fig. 6 as trace A, B, and C, which correspond to the open-circuit VMDP, the input-terminated VMDP, and the TLDP. We can clearly see that the input-terminated VMDP can achieve much better electrical bandwidth than the open-circuit VMDP (~330 GHz versus ~240 GHz), which is also close to the order of the cutoff frequency of the unit PD (~400 GHz), at the expense of one-half quantum efficiency. Compared with open-circuit VMDP, a significant improvement in the electrical bandwidth performance (~325 GHz), which is close to the bandwidth of the input-terminated VMDP, can be achieved with our proposed tapered structure without sacrificing the total quantum efficiency. In addition, the highest power bandwidth product can be expected in TLDP among these three structures.

IV. Conclusion

In this paper, we present the theory and design of a tapered line distributed photodetector. By utilizing the tapered line

structure and phase matching between optical waves and microwaves, a traveling-wave photodetector is more realizable and ultrahigh bandwidth can be attained without sacrificing quantum efficiency in the input dummy load. To investigate the advantages of TLDPs over VMDPs, both structures are simulated by a photodistributed current model, which is more analytical, intuitive, and can provide more physical insight than the traditional ABCD-matrix model. The chosen unit active PD in example TLDP and VMDP structures is LTG GaAs-based MSM TWPD for its high-speed and high-power performance. Both distributed structures in the bandwidth calculation are assumed to be transferred onto glass substrates so that the microwave radiation loss can be neglected. The simulated electrical bandwidth of the proposed TLDP is about 325 GHz, which is close to the simulated bandwidth of an input-terminated VMDP and higher than an input-open VMDP (240 GHz). The highest power-bandwidth product among these three structures can be achieved by the TLDP structure. This new design concept and structure can be applied to the high-bandwidth/power-distributed photodetectors for fiber radio communication systems, high-power photomixer devices [33], and low-cost photoreceiver circuits without electrical amplifiers [1].

ACKNOWLEDGMENT

The authors would like to thank Prof. M. J. W. Rodwell of the University of California, Santa Barbara, for stimulating technical discussions.

REFERENCES

[1] K. Kato, "Ultrawide-band/high-frequency photodetectors," *IEEE Trans. Microwave Theory Tech.*, vol. 47, pp. 1265–1281, 1999.

[2] V. M. Hietala, G. A. Vawter, T. M. Brenan, and B. E. Hammons, "Traveling-wave photodetectors for high-power, large bandwidth applications," *IEEE Trans. Microwave Theory Tech.*, vol. 43, pp. 2291–2297, 1995.

[3] S. Jasmin, N. Vodjdani, J. Renaud, and A. Enard, "Diluted- and distributed-absorption microwave waveguide photodiodes for high efficiency and high power," *IEEE Trans. Microwave Theory Tech.*, vol. 45, pp. 1337–1341, 1997.

[4] J.-W. Shi and C.-K. Sun, "Design and analysis of long-absorption length traveling-wave photodetector," *J. Lightwave Technol.*, vol. 18, pp. 2176–2187, 2000.

[5] L. Y. Lin, M. C. Wu, T. Itoh, T. A. Vang, R. E. Muller, D. L. Sivco, and A. Y. Cho, "High-power high-speed photodetectors design, analysis, and experiment demonstration," *IEEE Trans. Microwave Theory Tech.*, vol. 45, pp. 1320–1331, 1997.

[6] S. Murthy, T. Jung, T. Chau, M. C. Wu, D. L. Sivco, and A. Y. Cho, "Novel monolithic distributed traveling wave photodetector with parallel optical feed," *IEEE Photon. Technol. Lett.*, vol. 12, pp. 681–683, 2000.

[7] E. L. Ginzton, W. R. Hewlett, J. H. Jasberg, and J. D. Noe, "Distributed amplification," *Proc. IRE*, vol. 36, pp. 956–969, 1948.

[8] J.-W. Shi, K. G. Gan, Y. J. Chiu, Y.-H. Chen, C.-K. Sun, Y. J. Yang, and J. E. Bowers, "Metal–semiconductor–metal traveling-wave-photodetectors," *IEEE Photon. Technol. Lett.*, vol. 13, pp. 623–625, 2001.

[9] K. S. Giboney, Ph.D. dissertation, University of California at Santa Barbara, 1995.

[10] M. Y. Frankel, S. Gupta, J. A. Valdmanis, and G. A. Mourou, "Terahertz attenuation and dispersion characteristics of coplanar transmission lines," *IEEE Trans. Microwave Theory Tech.*, vol. 39, pp. 910–916, 1991.

[11] M. Y. Frankel, R. H. Voelker, and J. N. Hilfiker, "Coplanar transmission lines on thin substrates for high-speed low-loss propagation," *IEEE Trans. Microwave Theory Tech.*, vol. 42, pp. 396–402, 1994.

[12] T. T. Wong, *Fundamentals of Distributed Amplification*. Boston, MA: Artech House, 1993, ch. 7.

[13] M. P. Nesnidal, A. C. Davidson, G. R. Emmel, and R. A. Marsland, "Efficient, reliable, high-power VMDP's for linear fiber-optic signal transmission," in *Photonic Systems for Antenna Application Dig.*, 2000.

[14] S. Fukushima, C. F. C. Silva, Y. Muramoto, and A. J. Seeds, "InP–InGaAs uni-traveling-carrier photodiode with improved 3-dB bandwidth of over 150 GHz," *IEEE Photon. Technol. Lett.*, vol. 10, pp. 412–414, 1998.

[15] Y. Hirota, T. Hirono, T. Ishibashi, and H. Ito, "1.55-μm wavelength periodic traveling-wave photodetector fabricated using unitraveling-carrier photodiode structures," *J. Lightwave Technol.*, vol. 19, pp. 1751–1758, 2001.

[16] Y. J. Chiu, S. B. Fleischer, and J. E. Bowers, "High-speed low-temperature-grown GaAs p-i-n traveling-wave photodetector," *IEEE Photon. Technol. Lett.*, vol. 10, pp. 1012–1014, 1998.

[17] M. S. Islam, S. Murthy, T. Itoh, M. C. Wu, D. Novak, R. B. Waterhouse, D. L. Sivco, and A. Y. Cho, "Velocity-matched distributed photodetectors and balanced photodetectors with p-i-n photodiodes," *IEEE Trans. Microwave Theory Tech.*, vol. 49, pp. 1914–1920, 2001.

[18] S. Murthy, M. C. Wu, D. Sivco, and A. Y. Cho, "Parallel feed traveling wave distributed *pin* photodetectors with integrated MMI couplers," *Electron. Lett.*, vol. 38, pp. 78–80, 2002.

[19] K. Krishnamurthy, Ph.D. dissertation, University of California at Santa Barbara, 2000.

[20] E. S. Shapiro, J. Xu, A. S. Nagra, F. Williams, Jr., U. K. Mishra, and R. A. York, "A high-efficiency traveling-wave power amplifier topology using improved power-combining techniques," *IEEE Microwave Guided Wave Lett.*, vol. 8, pp. 133–135, 1998.

[21] J. J. Xu, Y.-F. Wu, S. Keller, G. Parish, S. Heikman, B. J. Thibeault, U. K. Mishra, and R. A. York, "1–8 GHz GaN based power amplifier using flip-chip bonding," *IEEE Microwave Guided Wave Lett.*, vol. 9, pp. 277–279, 1999.

[22] K. Krishnamurthy, S. I. Long, and M. J. W. Rodwell, "Cascode-delay-matched distributed amplifiers for efficient broadband microwave power amplification," in *IEEE 1999 Microwave Millimeter-Wave Monolithic Circuits Symp. Dig.*, 1999, pp. 819–822.

[23] J.-W. Shi, Y. H. Chen, K. G. Gan, Y. J. Chiu, C.-K. Sun, and J. E. Bowers, "High speed and high power performances of LTG-GaAs based metal–semiconductor–metal traveling-wave-photodetectors in 1.3 μm wavelength regime," *IEEE Photon. Technol. Lett.*, vol. 14, pp. 363–365, 2002.

[24] J.-W. Shi, K. G. Gan, Y. J. Chiu, and J. E. Bowers, "High power performance of ultrahigh bandwidth MSM TWPDs," in *Conf. Proc. IEEE Lasers Electro-Optics Society 2001 Annu. Meeting*, vol. 2, 2001, pp. 887–888.

[25] K. C. Gupta, R. Garg, I. Bahl, and P. Bhartia, *Microstrip Lines and Slotlines*. Boston, MA: Artech House, 1996.

[26] A. A. Omar, Y. L. Chow, L. Roy, and M. G. Stubbs, "Effects of air-bridge and mitering on coplanar waveguide 90° bends: Theory and experiment," in *IEEE MTT-S Dig.*, 1993, pp. 823–826.

[27] J. Lee, J. Kim, S. Yu, and J. Kim, "Picosecond time-domain characterization of CPW bends using a photoconductive near-field mapping probe," *IEEE Microwave Wireless Components Lett.*, vol. 11, pp. 453–455, 2001.

[28] D. M. Pozar, *Microwave Engineering*. New York: Wiley, 1998.

[29] S. S. Bedair and I. Wolff, "Fast, accurate and simple approximate analytic formulas for calculating the parameters of supported coplanar waveguides for (M)MIC's," *IEEE Trans. Microwave Theory Tech.*, vol. 40, pp. 41–48, 1992.

[30] Y. R. Kwon, V. M. Hietala, and K. S. Champlin, "Quasi-TEM analysis of 'slow-wave' mode propagation on coplanar microstructure MIS transmission lines," *IEEE Trans. Microwave Theory Tech.*, vol. MTT-35, pp. 545–551, 1987.

[31] M. J. W. Rodwell, S. T. Allen, R. Y. Yu, M. G. Case, U. Bhattacharya, M. Reddy, E. Carman, M. Kamegawa, Y. Konishi, J. Pusl, and R. Pullela, "Active and nonlinear wave propagation devices in ultrafast electronics and optoelectronics," *Proc. IEEE*, vol. 82, pp. 1037–1059, 1994.

[32] R. J. Deri and E. Kapon, "Low-loss III–V semiconductor optical waveguides," *IEEE J. Quantum Electron.*, vol. 27, pp. 626–640, 1991.
[33] S. Gupta, J. F. Whitaker, and G. A. Mourou, "Ultrafast carrier dynamics in III–V semiconductors grown by molecular-beam epitaxy at very low substrate temperatures," *IEEE J. Quantum Electron.*, vol. 28, pp. 2464–2472, 1992.
[34] A. Hirata, H. Ishii, and T. Nagatsuma, "Design and characterization of a 120-GHz millimeter-wave antenna for integrated photonic transmitters," *IEEE Trans. Microwave Theory Tech.*, vol. 49, pp. 2157–2162, 2001.

Jin-Wei Shi, photograph and biography not available at the time of publication.

Chi-Kuang Sun (M'96–SM'01), photograph and biography not available at the time of publication.